Supplement of Biogeosciences, 11, 6827–6840, 2014
http://www.biogeosciences.net/11/6827/2014/
doi:10.5194/bg-11-6827-2014-supplement

Biogeosciences Open Access

Supplement of

Local spatial structure of forest biomass and its consequences for remote sensing of carbon stocks

M. Réjou-Méchain et al.

Correspondence to: M. Réjou-Méchain (maxime.rejou@gmail.com)

SUPPLEMENT

Supplement S1: Analyzing the spatial structure in AGBD with wavelet analysis

To investigate the contribution of variation at different scales to the spatial structure of AGBD within field plots, we used wavelet-kernel functions (Percival, 1995). The wavelet transform analyzes the variance across spatial scales *s* by decomposing the signal into an orthonormal wavelet basis. The wavelet transform is defined as

$$W_f(\boldsymbol{b}, s, \theta) = s^{-1} \int f(\boldsymbol{x}') \phi_s^*(\boldsymbol{x}' - \boldsymbol{b}) d\boldsymbol{x}'$$

where $f(\boldsymbol{x})$ is the raster of the AGBD at the smallest field resolution (5 m x 5 m pixel), $\phi_s^*(\boldsymbol{x} - \boldsymbol{b})$ is the complex conjugate of the scaled and translated mother wavelet, *s* is the scale at which the transform is applied, and $\boldsymbol{b}$ is the translation vector. The convolution is efficiently computed using fast Fourier routines. We used an isotropic Morlet wavelet, with Fourier transform given by

$$\hat{\phi}_s = \frac{s}{c_\phi} \exp\left[-\frac{1}{2} \left(s\boldsymbol{k} - k_0 \right)^2 \right]$$

The functions ∅ are essentially band-pass filters whose properties depend on the associated scaling parameter, *s*. They enable a focus on features of the process whose detail matches their scale parameters, i.e., broad features for large *s* and fine features for small *s*. We compute the wavelet variance or spectrum, $S_{ff}(s)$, as

$$S_{ff}(s, \theta) = \int_A |W_f(\boldsymbol{b}, s)|^2 \, d\boldsymbol{b}$$

We then normalized by the total variance to obtain the normalized wavelet variances.

Supplement S2: An alternative reliability study approach

In this reliability study, we assumed that additional subplots (i.e. replicates) of 0.04 ha (n=19), 0.1 ha (n=9), 0.25 ha (n=4), 0.5 ha (n=2), 1 ha (n=1) and 2 ha (n=1) were established randomly inside the 4-ha pixel. The numbers of additional subplots were chosen to be realistic and increasing these numbers did not substantially affect the results (not shown). Two cases were simulated: additional subplots did not overlap each other or with the original subplot ("Replicate *Rr*") or additional subplots were allowed to overlap each other or the original subplot ("Replicate *Rr* Overlap"). The original subplot and the replicates were then used to calculate the ICC considering the 4-ha pixel as factor in the one-way analysis of variance (see methods). Results showed that "Replicate *Rr*" tended to overestimate the correction needed for all subplot areas, while the "Replicate *Rr* Overlap" overestimated the correction needed for small subplot and underestimated the correction for larger subplot areas (Fig. S3). In all cases, these corrections did not outperform the "within subplot *Rr*" bootstrap approach for a given surveyed area.

FIGURES

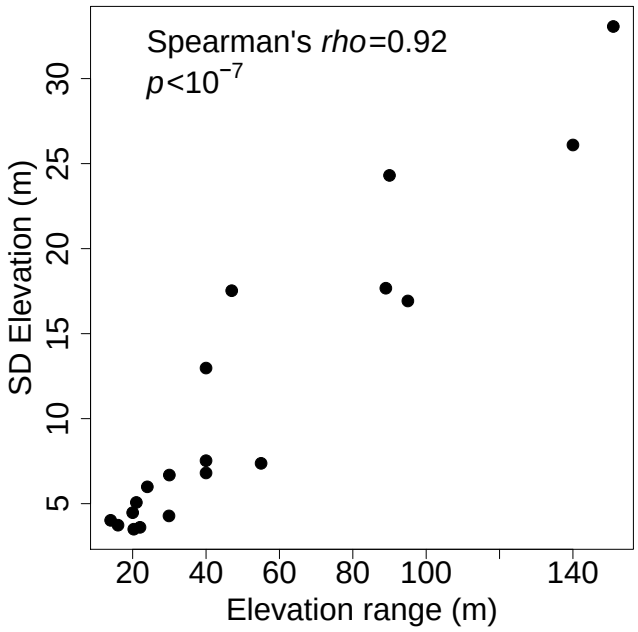

Figure S1. Relation between the elevation range and the mean standard deviation (SD) of elevation within 1-ha subplots in 19 study sites. Because elevation range is dependent not only upon topographical variability but also on plot size, we examined how elevation range correlated with a plot-size-independent measure of topographical variability, specifically the mean standard deviation of elevation within 1-ha subplots. Pearson's correlation test results are given within the panel. The SD of elevation was calculated for each discrete 1-ha within each plot from elevation maps of 20 m resolution, and then averaged over 1-ha subplots within each plot (the SD of elevation was almost insensitive to the resolution grain size, result not shown). All sites for which elevation maps were available were included in this analysis (Amacayacu, Barro Colorado Island, Fushan, Haliburton, Huai Kha Khaeng, Ituri Edoro1, Ituri Edoro2, Ituri Lenda1, Ituri Lenda2, Korup, Luquillo, Manaus, Mudumalai, Nouragues, Palanan, Paracou, Pasoh, Sinharaja, Yasuni).

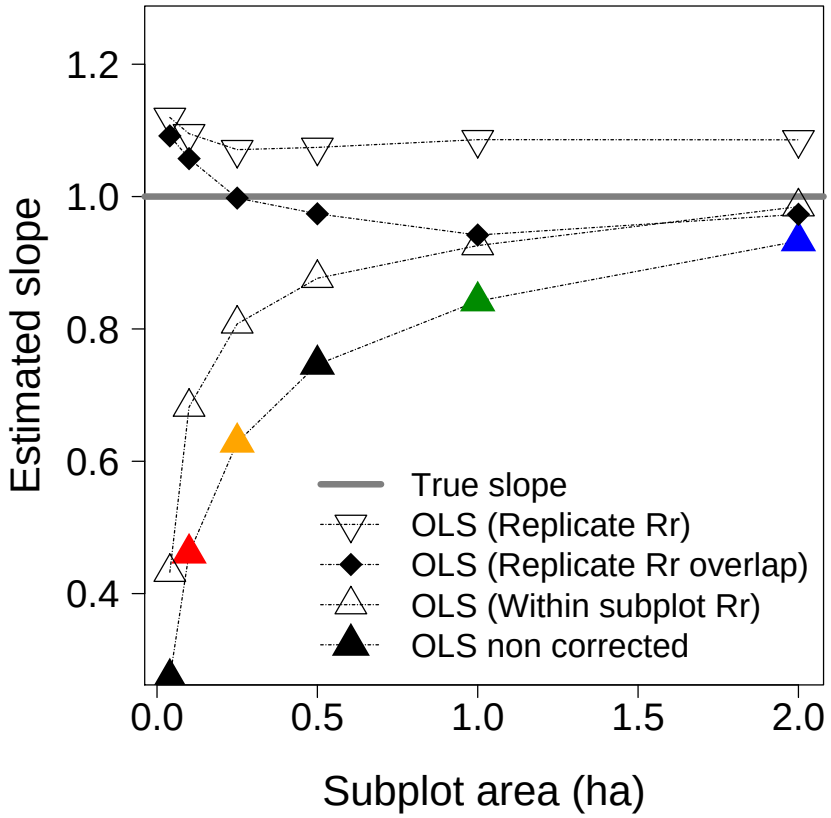

Figure S2. Effects on estimated regression slopes of an alternative reliability study approaches employing additional subplots established randomly inside the 4-ha pixel (Appendix S2). See Appendix S2 and figure 7 of the main manuscript for details.

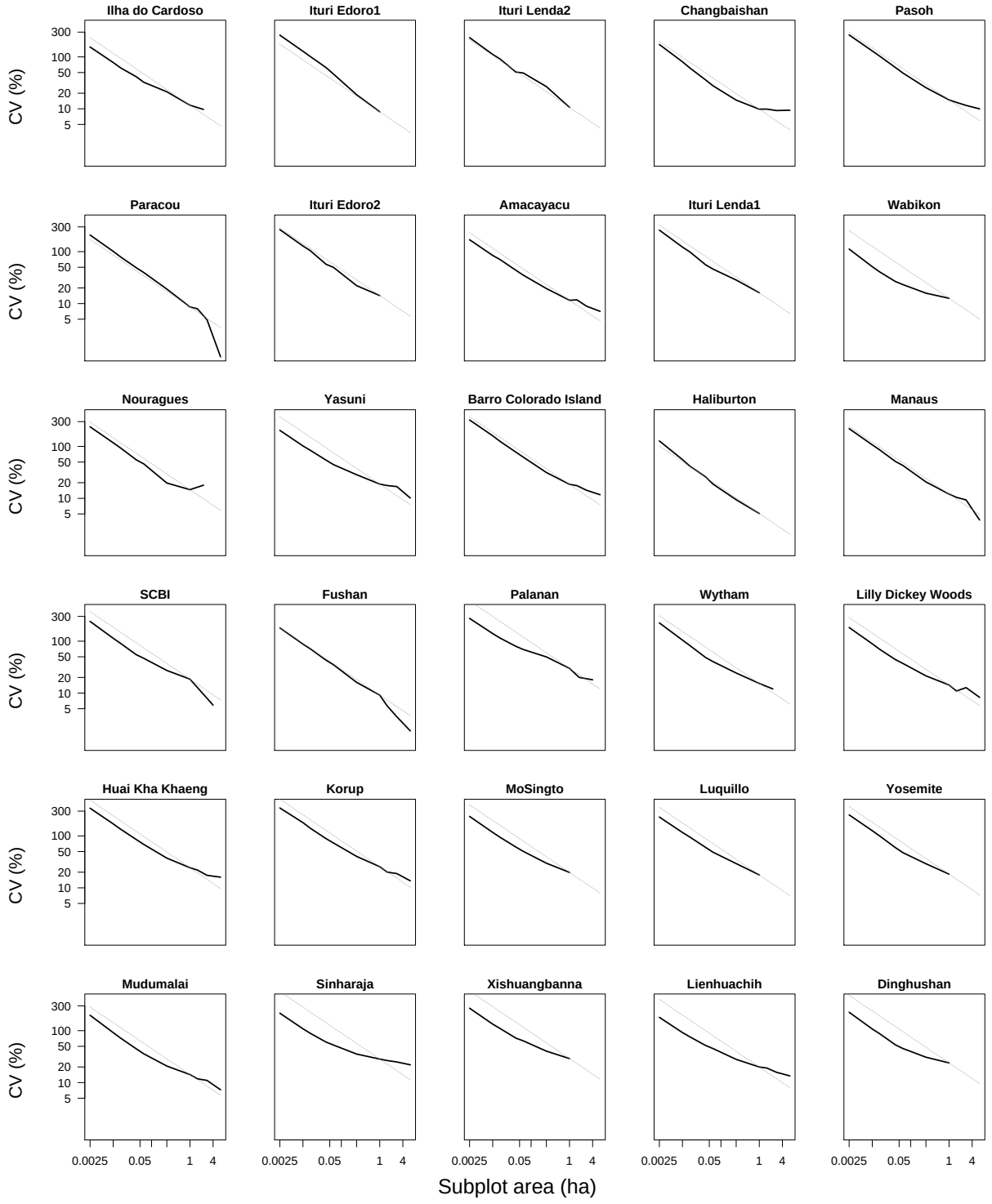

Figure S3. Spatial variation in AGBD as a function of spatial scale within each site. The coefficient of variation (CV) of AGBD among subplots is plotted as a function of subplot area, with both on log scales. The grey dotted lines represent the fitted theoretical lines expected if no spatial autocorrelation occurs and CVs at any scale can be predicted from $CV(1)$, the observed CV at 1-ha scales, as $CV(s) = CV(1) \times s^{-\frac{1}{2}}$. Panels are ordered by elevation range.

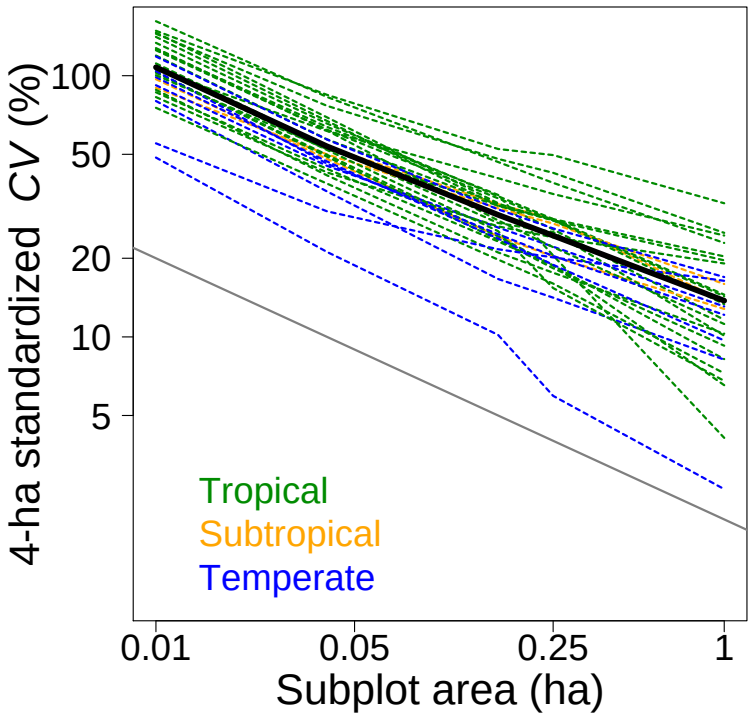

Figure S4. Local spatial variability in AGBD within 4-ha subplots at each site (one dashed line per site) and the mean over all sites (solid black line) as a function of spatial scale. For each site, the spatial variability at a given spatial scale was quantified as the mean coefficient of variation (CV) of AGBD for square subplots that gridded entire 4-ha subplots, with the mean taken over 1000 randomly placed 4-ha subplots. The rate of decline deviated somewhat from the slope of -0.5 (on log-log scales) expected in the absence of spatial autocorrelation in AGBD (solid grey reference line).

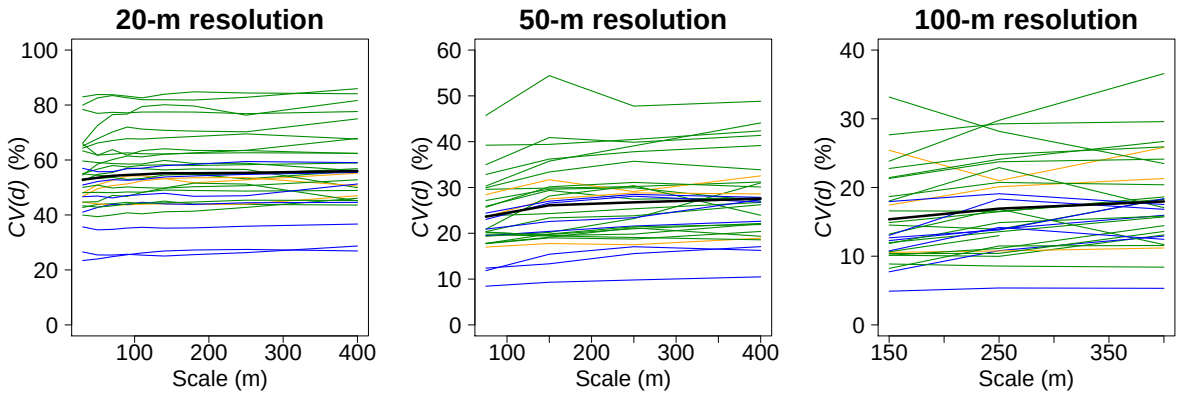

Figure S5. Variograms for AGBD in square subplots of 20, 50 and 100-m resolution for each site (colored lines) together with the average across sites (thick black line). Variances were transformed into distance-specific coefficients of variation (CV(d); see methods). Line color indicates forest type as in Fig. S4: tropical (green), subtropical (orange) and temperate (blue). To best represent the variability at each spatial resolution, the scale of the y-axis changes between panels.

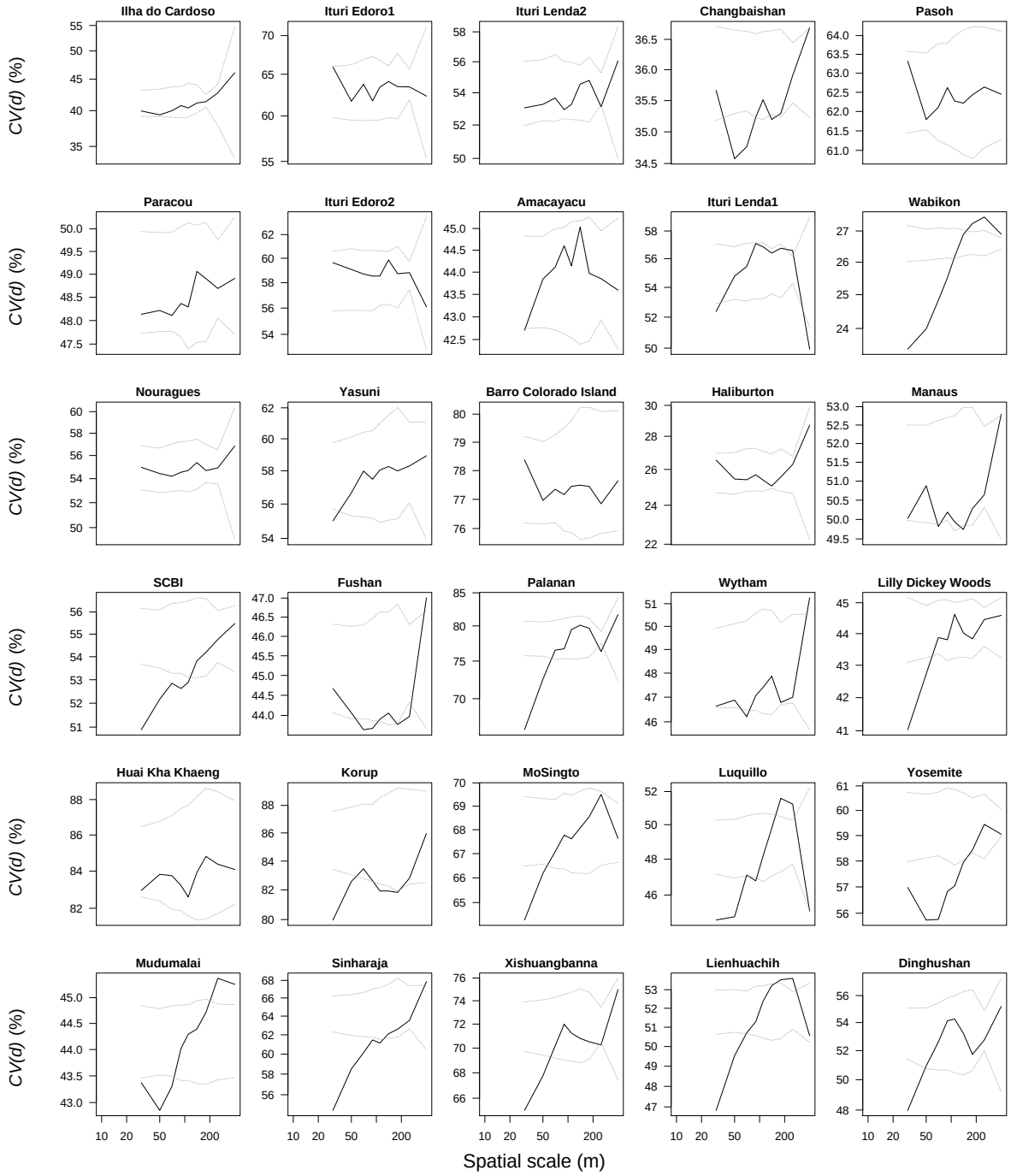

Figure S6. Variograms for AGBD in 20 x 20 m (0.04 ha) quadrats, for each site. For comparison purpose, variances were transformed into distance-specific coefficients of variation (CV(d); see methods). The grey dotted lines show the 95% confidence intervals on the null hypothesis of no spatial autocorrelation, as computed from 500 permutations (data values were randomly assigned to spatial locations). Panels are ordered by elevation range. Note that the y axis varies among panels.

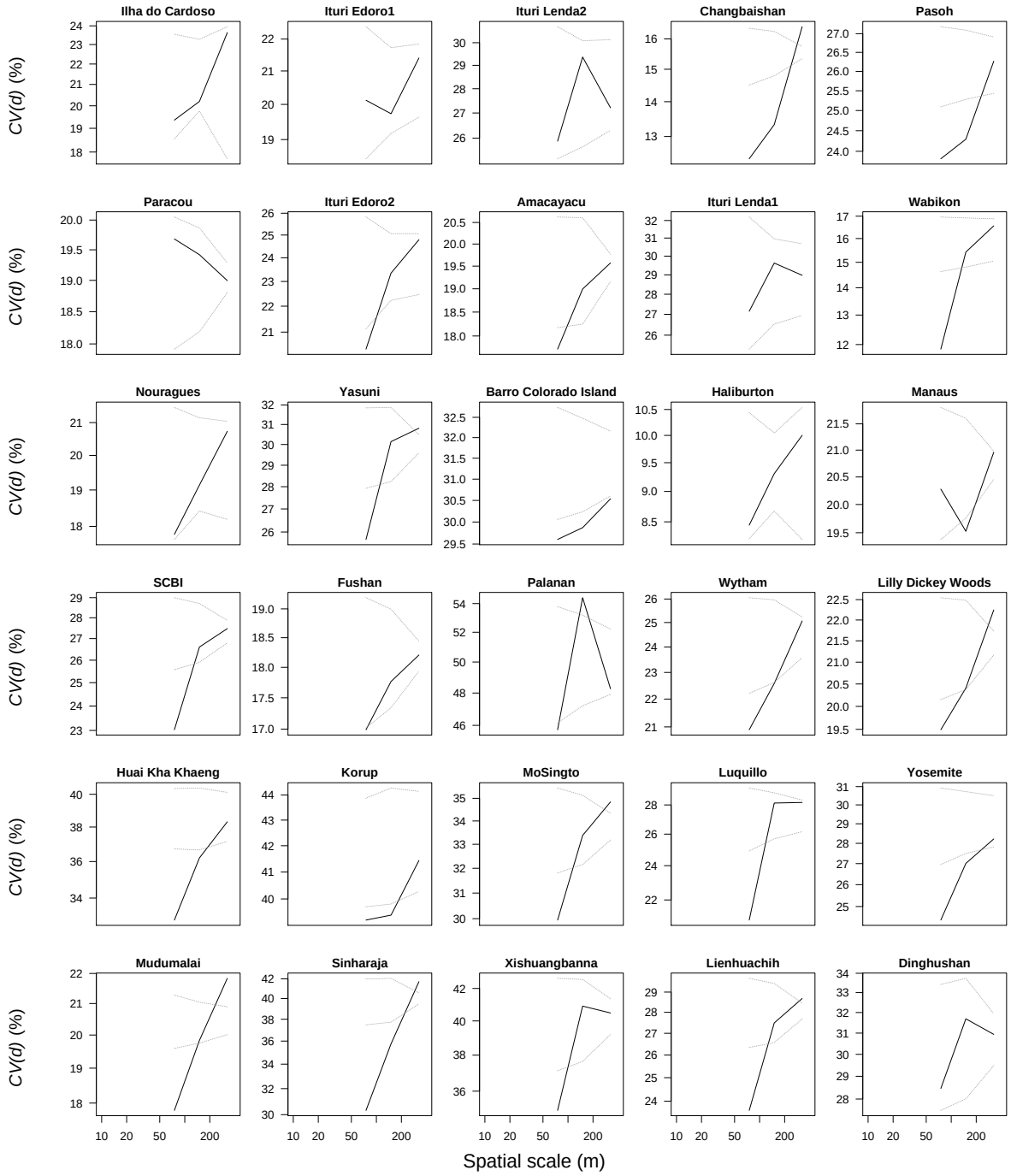

Figure S7. Variograms for AGBD in 50 x 50 m (0.25 ha) quadrats, for each site. For comparison purpose, variances were transformed into distance-specific coefficients of variation (CV(d); see methods). The grey dotted lines show the 95% confidence intervals on the null hypothesis of no spatial autocorrelation, as computed from 500 permutations (data values were randomly allocated to the spatial locations). Panels are ordered by elevation range. Note that the y axis varies among panels.

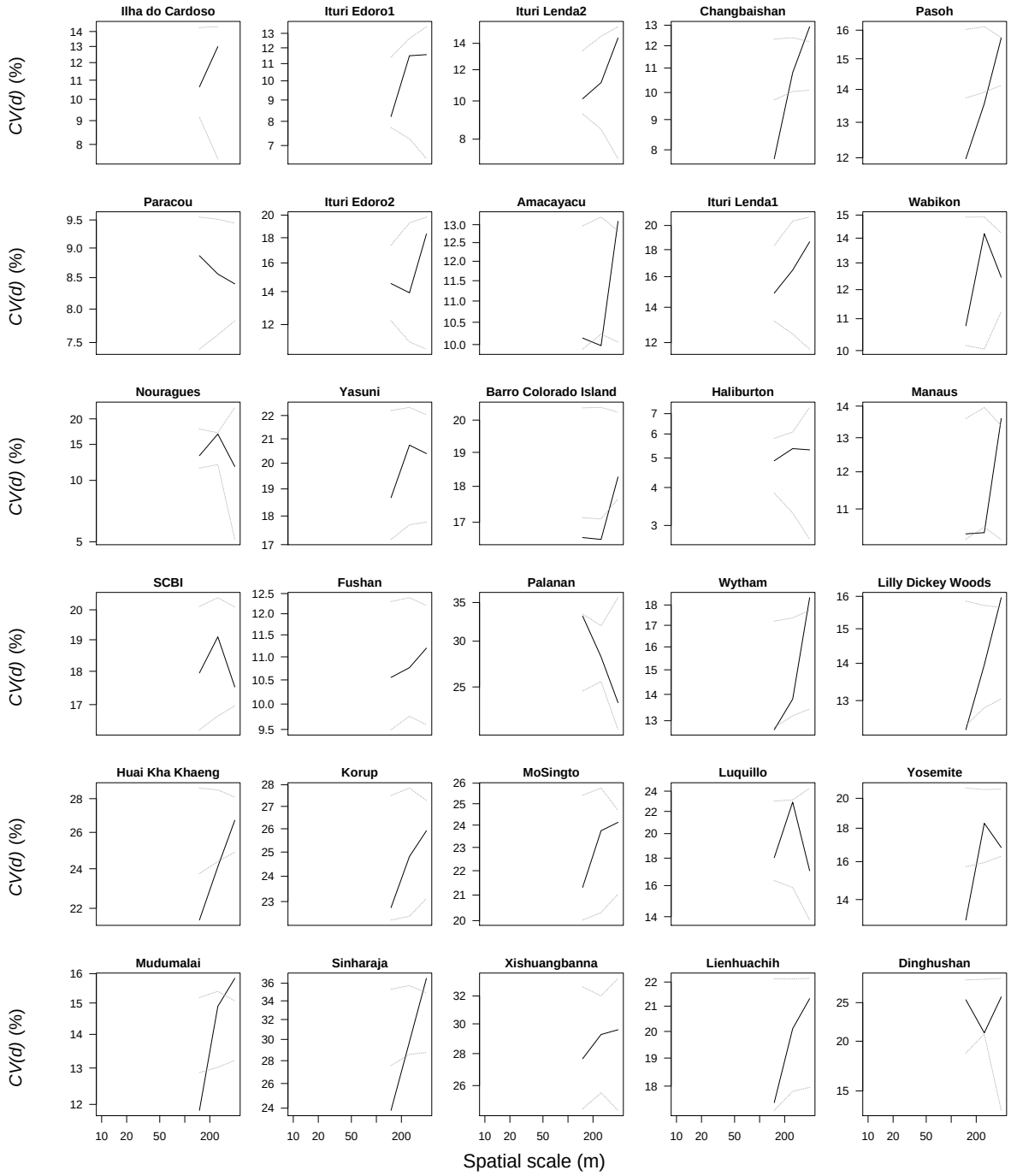

Figure S8. Variograms for AGBD in 100 x 100 m (1 ha) quadrats, for each site. For comparison purpose, variances were transformed into distance-specific coefficients of variation (CV(d); see methods). The grey dotted lines show the 95% confidence intervals on the null hypothesis of no spatial autocorrelation, as computed from 500 permutations (data values were randomly allocated to the spatial locations). Panels are ordered by elevation range. Note that the y axis varies among panels.

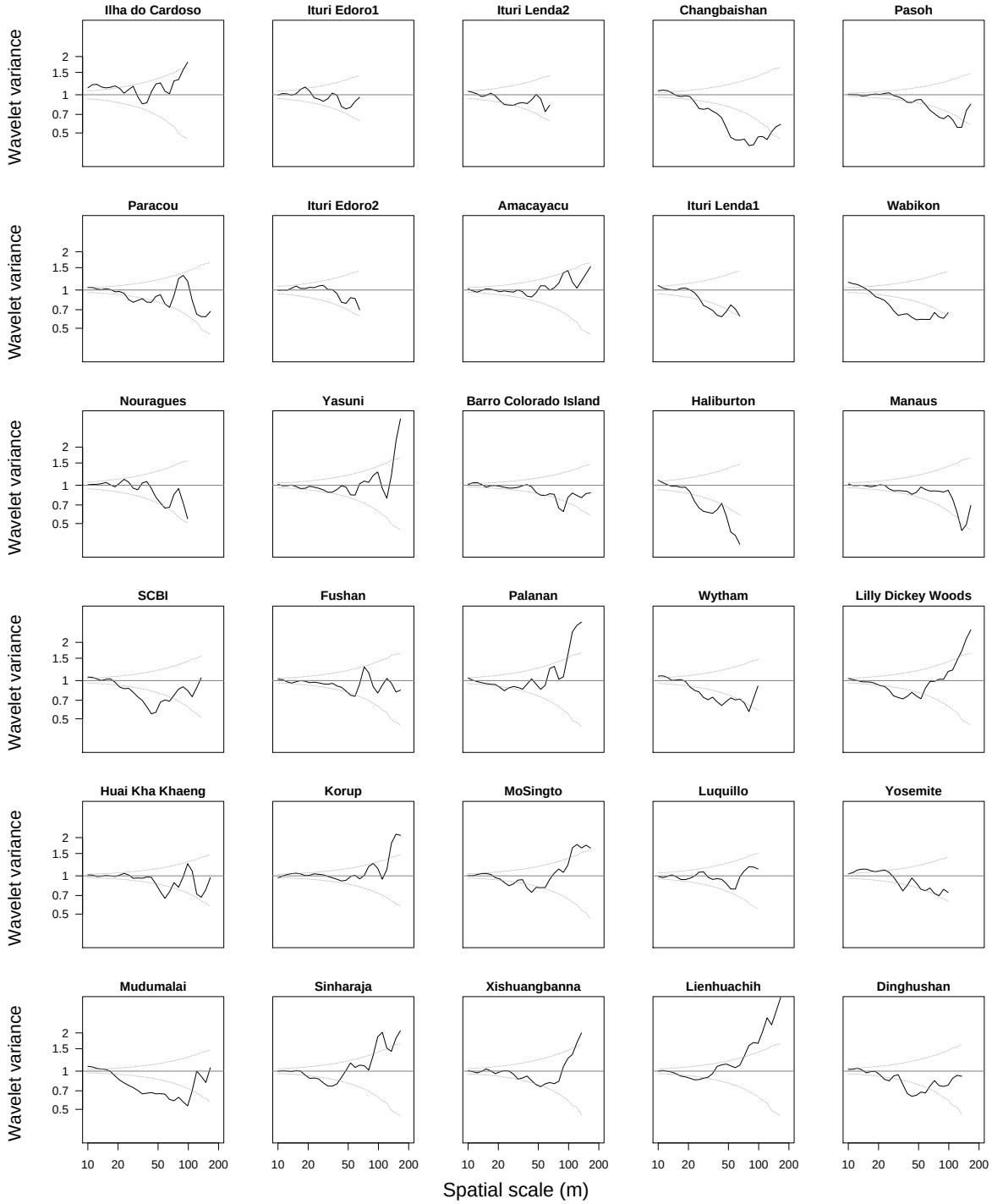

Figure S9. Scale-wise decomposition of spatial variation in AGBD within each site. The normalized wavelet variance computed for each site (solid black line) is contrasted with the value of 1 expected under no spatial structure (solid grey line). A higher wavelet variance indicates aggregation or clustering at a specific spatial scale (period), while a lower variance indicates dis-aggregation. The grey dotted lines show the 95% confidence intervals on the null hypothesis of no spatial structure, as computed from a chi-square distribution with *k* degrees of freedom, where *k* depends on the total area and the considered spatial scale. Panels are ordered by elevation range.

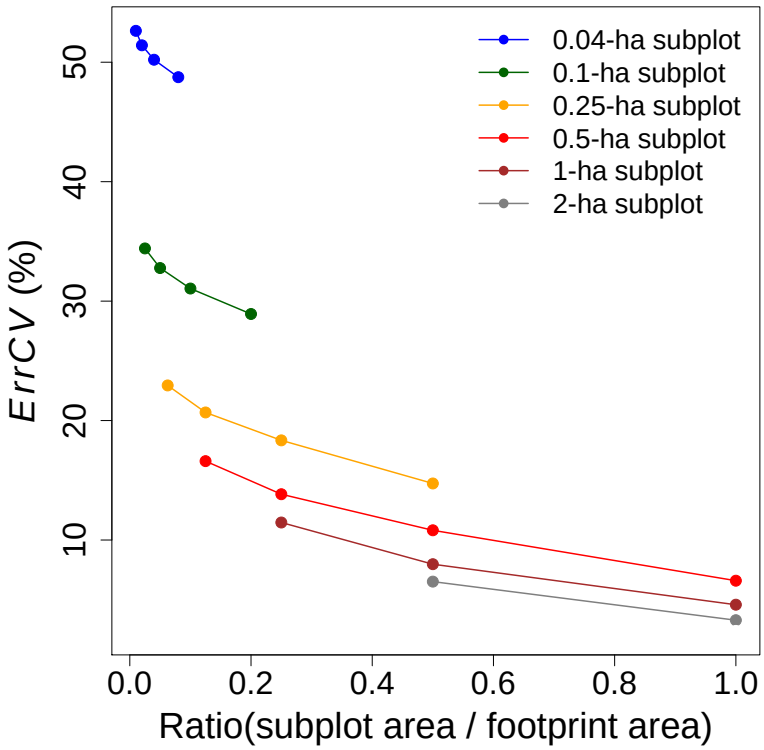

Figure S10. The mean error coefficient of variation (*ErrCV*) in AGBD as a function of the ratio of the subplot area to the remote sensing resolution for different subplot areas (see key). As illustrated here, for a same ratio of the field calibration plot area to the footprint area on the x axis, i.e. a same spatial representativeness of the subplot, the error due to the spatial mismatch is higher for small calibration plots. This figure is based on the simulation scheme described in figure 2.

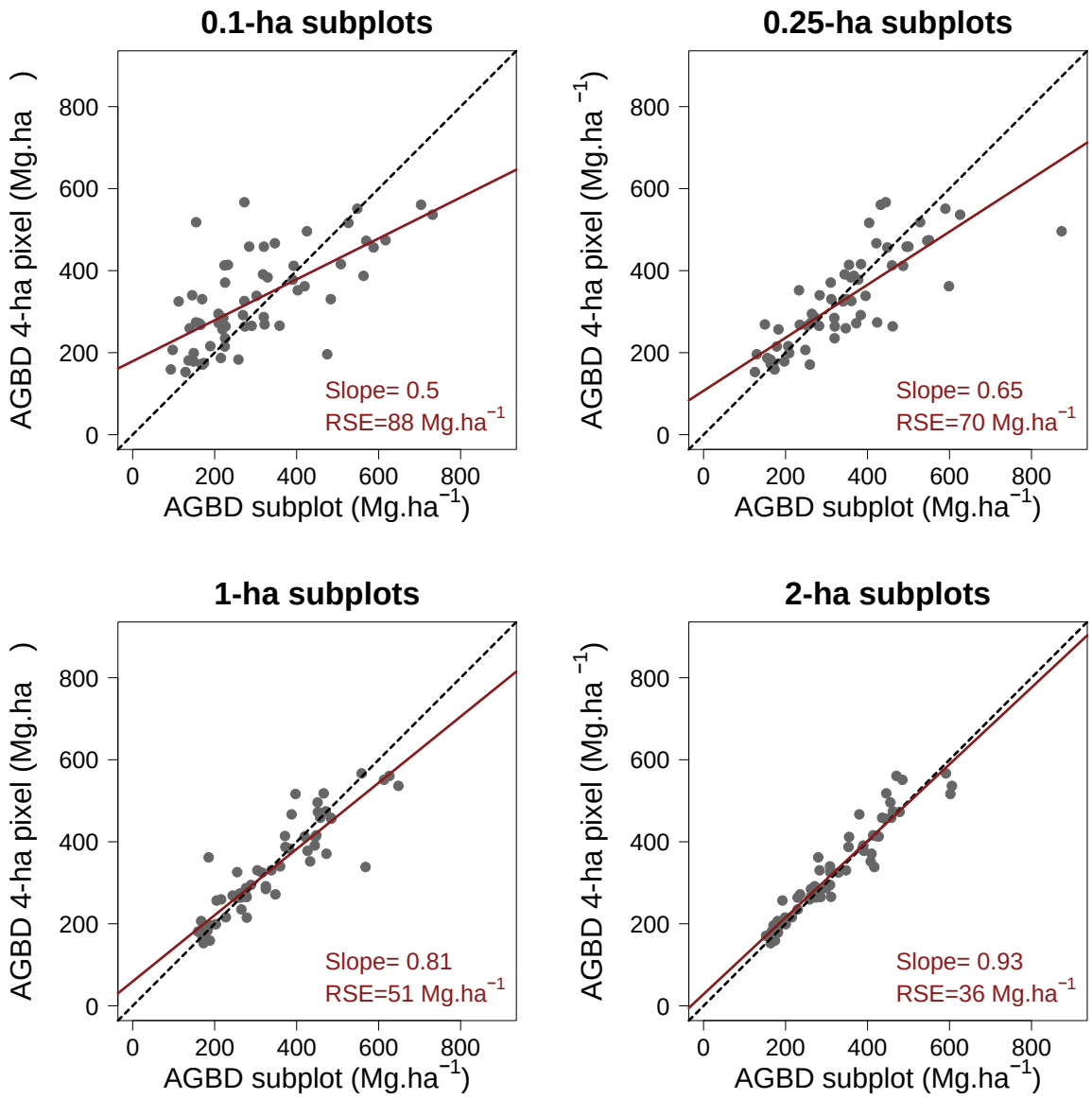

Figure S11. Propagation of field sampling errors to remote sensing products: an example randomly drawn from the 1,000 simulations. Panels illustrate the AGBD estimated within two 4-ha pixels randomly established in each large plot (n=60, dependent variable) and variable-size subplots located within the 4-ha pixels (independent variable). The regression line obtained from an OLS linear regression between the two AGBD estimates is shown on each figure (red line). The slope and the residual standard error (RSE) of the model are given in the key. The true slope is one (black dotted line).

TABLES

Table S1. Study site characteristics.

Site	Country	Continent	Lat	Long	Plotdim (m)	Area (ha)	Forest type‡	Elevation range (m)	Minimum dbh (cm)	Census year	*WSG* values§	Allometry used§	AGBD ($Mg.ha^{-1}$)
Amacayacu	Colombia	America	-3.80917	-70.2679	500x500	25	Tropical	22	1	2011	1	2	203.0
Barro Colorado Island	Panama	America	9.1543	-79.8461	1000x500	50	Tropical	40	1	2010	1	2	302.7
Changbaishan	China (Jilin)	Asia	42.3833	128.083	500x500	25	Temperate	17.7	1	2009	-	3	276.9
Dinghushan	China (Guangdong)	Asia	23.1695	112.511	400x500	20	Subtropical	240	1	2005	1	2	249.6
Fushan	Taiwan	Asia	24.7614	121.555	500x500	25	Subtropical	47	1	2009	1	2	175.2
Haliburton	Canada (Ontario)	America	45.2901	-78.6377	400x200*	8	Temperate	50.9	1	2008	-	4	175.5
Huai Kha Khaeng	Thailand	Asia	15.6324	99.217	1000x500	50	Tropical	89	1	2009	1	2	399.1
Ilha do Cardoso	Brazil (São Paulo)	America	-25.0955	-47.9573	300x300*	9	Tropical	5	1	2009	1	2	276.7
Ituri Edoro1	Democratic Republic of Congo	Africa	1.4368	28.5826	200x500	10	Tropical	14	1	2007	1	2	436.5
Ituri Edoro2	Democratic Republic of Congo	Africa	1.4368	28.5826	200x500	10	Tropical	21	1	2007	1	2	432.7
Ituri Lenda1	Democratic Republic of Congo	Africa	1.4368	28.5826	200x500	10	Tropical	24	1	2007	1	2	542.1
Ituri Lenda2	Democratic Republic of Congo	Africa	1.4368	28.5826	200x500	10	Tropical	16	1	2007	1	2	555.4
Korup	Cameroon	Africa	5.07389	8.85472	1000x500	50	Tropical	90	1	2009	1	2	361.8
Lienhuachih	Taiwan	Asia	23.9136	120.879	500x500	25	Subtropical	174	1	2007	1	2	188.6
Lilly Dickey Woods	USA (Indiana)	America	39.2361	-86.2204	500x500	25	Temperate	72	1	2012	-	4	267.8
Luquillo	Puerto Rico	America	18.3262	-65.816	300x500*	15	Tropical	95	1	2000	1	2	358.0
Manaus	Brazil (Amazonas)	America	-2.4417	-59.7858	500x500	25	Tropical	40	1	2007	1	2	322.5
Mo Singto	Thailand	Asia	14.4333	101.35	600x500	30	Tropical	90	1	2005	1	2	310.1
Mudumalai	India (Tamil Nadu)	Asia	11.5989	76.5338	1000x500	50	Tropical	140	1	1992	1	2	172.0
Nouragues	French Guiana	America	4.091944	-52.67861	300x400	12	Tropical	29.9	10	2008	1	2	391.5
Palanan	Philippines	Asia	17.0402	122.388	400x400	16	Tropical	55	1	2010	1	2	444.6
Paracou	French Guiana	America	5.25	-52.91667	500x500	25	Tropical	20.3	10	2009	1	2	405.4
Pasoh	Malaysia	Asia	2.982	102.313	1000x500	50	Tropical	20	1	1990	1	2	336.9
SCBI: Smithsonian Conservation Biology Institute	USA (Virginia)	America	38.8916	-78.1457	400x600*	24	Temperate	43	1	2008	-	4	255.0
Sinharaja	Sri Lanka	Asia	6.4023	80.4023	500x500	25	Tropical	151	1	2002	1	2	563.9
Wabikon Lake Forest	USA (Wisconsin)	America	45.5508	-88.7964	300x800*	24	Temperate	25.9	1	2008	-	4	179.9
Wytham woods	UK	Europe	51.7743	-1.3379	300x600	18	Temperate	60	1	2010	-	5	195.5
Xishuangbanna	China (Yunnan)	Asia	21.6117	101.574	400x500	20	Tropical	160	1	2007	1	2	424.7
Yasuni	Ecuador	America	-0.6859	-76.3953	500x500	25	Tropical	30	1	2002	1	2	285.2
Yosemite National Park	USA (California)	America	37.7662	-119.819	800x300*	24	Temperate	137.2	1	2010	-	6	545.8

* Only a subset of the plot of these dimensions was employed in our analyses, some of which required that both plot dimensions be multiples of 100.

§ 1-Chave *et al.* (2009); 2-Chave *et al.* (2005); 3-Wang *et al.* (2006); 4-Jenkins *et al.* (2003); 5-see Fenn *et al.* (2010); 6-Lutz *et al.*. (2012)

‡ Forest types were derived from Fischer et al. (2012) but due to its high elevation, the Yosemite forest has been considered as a temperate forest, instead of a subtropical one (see Fig.1 of the paper).

Table S2. Coefficient of variation (CV) of AGBD (in %) according to subplot size in each study plot. The mean CV across plots is given at the end of the table for each subplot size.

Field plots	**5 m x 5 m**	**10 m x 10 m**	**12.5 m x 12.5 m**	**20 m x 20 m**	**25 m x 25 m**	**50 m x 50 m**	**100 m x 100 m**	**125 m x 125 m**	**166.7 m x 166.7 m**	**250 m x 250 m**
Amacayacu	169.51	84.44	70.18	43.84	35.28	19.45	11.58	11.78	8.90	7.09
Barro Colorado Island	322.79	160.09	124.57	77.70	62.14	31.40	18.62	17.57	14.30	11.75
Changbaishan	173.17	80.42	61.12	36.03	27.74	14.71	9.83	9.88	9.26	9.39
Dinghushan	226.08	107.61	87.27	53.36	45.42	30.82	23.96	-	-	-
Fushan	180.30	87.81	71.00	42.96	35.16	16.07	9.14	5.66	3.50	1.87
Haliburton	127.33	55.66	41.52	25.93	18.79	9.40	5.10	-	-	-
Huai Kha Khaeng	341.81	170.43	134.84	85.07	68.59	37.33	24.38	22.02	17.41	16.03
Ilha do Cardoso	155.28	78.01	61.45	41.47	32.50	21.30	11.74	-	-	-
Ituri Edoro1	262.68	128.47	101.42	62.22	46.66	18.69	8.77	-	-	-
Ituri Edoro2	265.75	128.64	104.02	57.08	49.75	22.15	14.26	-	-	-
Ituri Lenda1	259.95	122.20	98.72	55.87	46.12	28.41	16.17	-	-	-
Ituri Lenda2	235.01	111.42	90.92	51.11	48.99	26.81	10.68	-	-	-
Korup	345.59	180.31	140.24	88.67	72.99	40.27	25.53	20.08	18.82	13.66
Lienhuachih	180.23	91.86	75.91	51.87	45.19	28.01	19.97	19.11	15.83	13.46
Lilly Dickey Woods	183.16	88.83	69.62	44.20	37.29	21.45	14.30	10.98	12.73	8.26
Luquillo	230.76	116.36	94.81	60.07	48.53	29.29	17.73	-	-	-
Manaus	219.60	107.05	85.76	51.31	42.96	20.71	12.06	10.43	9.32	3.82
MoSingto	237.24	116.74	93.95	61.06	50.37	29.82	19.81	-	-	-
Mudumalai	197.80	91.78	71.85	44.61	35.90	20.83	14.27	11.83	11.01	7.27
Nouragues	238.87	117.52	93.16	55.09	46.15	19.72	14.69	-	-	-
Palanan	274.28	139.79	114.34	79.58	69.03	49.74	29.93	-	-	-
Paracou	209.01	101.47	79.08	48.94	39.66	19.03	8.61	7.95	4.89	0.94
Pasoh	264.98	130.06	103.31	62.52	49.04	25.54	14.85	13.29	11.63	9.98
SCBI	240.22	113.79	90.52	54.86	46.78	27.28	18.56	-	-	-
Sinharaja	216.91	108.54	88.76	60.25	52.82	35.42	28.39	26.58	24.98	22.01
Wabikon	112.08	51.30	40.66	26.59	23.24	15.87	12.63	-	-	-
Wytham	224.59	104.72	82.15	48.47	40.33	24.35	15.34	-	-	-
Xishuangbanna	270.57	133.49	109.81	71.85	63.58	40.28	29.03	-	-	-
Yasuni	203.75	102.22	83.93	54.36	44.61	28.48	18.80	17.61	16.86	10.13
Yosemite	254.02	125.91	99.44	59.47	47.68	29.09	18.33	-	-	-
MEAN	**227.44**	**111.23**	**88.81**	**55.21**	**45.78**	**26.06**	**16.57**	**14.63**	**12.82**	**9.69**

Table S3. Coefficients of the linear regression of the logarithm of the coefficient of variation, CV, in AGBD against the logarithm of plot area for each site. In the absence of spatial autocorrelation in AGBD, $CV(s) = CV(1)/s^{\gamma}$ with γ =½. Positive spatial autocorrelation should yield γ <½; negative spatial autocorrelation γ >½. Slopes that are significantly different from ½ are highlighted in bold; those that are significantly higher with bold italics.

Site	R^2	Intercept	γ	CI γ
Amacayacu	0.997	2.374	**0.45**	0.421-0.479
Barro Colorado Island	0.997	2.837	0.482	0.451-0.513
Changbaishan	0.986	2.102	0.489	0.421-0.557
Dinghushan	0.954	2.951	**0.375**	0.280-0.471
Fushan	0.998	2.153	0.505	0.481-0.528
Haliburton	0.996	1.532	0.539	0.499-0.579
Huai Kha Khaeng	0.992	3.068	**0.447**	0.401-0.493
Ilha do Cardoso	0.993	2.413	**0.423**	0.381-0.464
Ituri Edoro1	0.997	2.195	***0.576***	0.543-0.610
Ituri Edoro2	0.993	2.526	0.502	0.452-0.552
Ituri Lenda1	0.988	2.677	0.461	0.403-0.519
Ituri Lenda2	0.992	2.451	0.497	0.446-0.548
Korup	0.994	3.135	**0.441**	0.401-0.480
Lienhuachih	0.983	2.866	**0.365**	0.310-0.419
Lilly Dickey Woods	0.987	2.519	**0.426**	0.369-0.484
Luquillo	0.993	2.787	**0.428**	0.388-0.468
Manaus	0.998	2.413	0.49	0.462-0.518
Mo Singto	0.988	2.858	**0.415**	0.363-0.467
Mudumalai	0.982	2.483	0.442	0.372-0.511
Nouragues	0.986	2.506	0.485	0.420-0.551
Palanan	0.982	3.336	**0.355**	0.299-0.411
Paracou	1	2.186	***0.529***	0.516-0.541
Pasoh	0.997	2.611	0.487	0.455-0.519
SCBI: Smithsonian Conservation Biology Institute	0.982	2.758	**0.429**	0.362-0.496
Sinharaja	0.958	3.151	**0.338**	0.256-0.419
Wabikon Lake Forest	0.943	2.305	**0.359**	0.258-0.461
Wytham woods	0.983	2.582	0.447	0.381-0.514
Xishuangbanna	0.976	3.215	**0.369**	0.303-0.436
Yasuni	0.986	2.811	**0.396**	0.342-0.451
Yosemite National Park	0.987	2.774	0.442	0.384-0.500

Table S4. Topographic structure of the world ecological zones by continents. Metrics were calculated using maps at 3 arc minutes of resolution (~5.6 km²). The global ecological zoning of the FAO (2001) was used to classify ecological zones. Slope and elevation were estimated from the SRTM 30+ / ETOPO1 Global Relief Model (Amante & Eakins, 2009) and continents were assigned based on the global administrative area (http://www.gadm.org/). All these analyses were conducted with the R statistical software (R Development Core Team, 2012) using freely available global maps provided by the spatial-analyst.net project (http://spatial-analyst.net/).

FAO Ecological zones	**Africa**				**Asia**				**Europe**				**North America**			
	% of cover	Mean elevation	Mean slope	% of steep slope*	% of cover	Mean elevation	Mean slope	% of steep slope*	% of cover	Mean elevation	Mean slope	% of steep slope*	% of cover	Mean elevation	Mean slope	% of steep slope*
Polar					8.8	197	0.004	19	0.1	224	0.010	65	38.7	946	0.005	20
Boreal coniferous forest					16	218	0.003	8	15.9	253	0.005	23	8.1	416	0.003	13
Boreal mountain system					12.5	731	0.013	72	8.8	640	0.015	73	5.8	945	0.018	81
Boreal tundra woodland					5	310	0.007	36		156	0.005	31	11.4	315	0.004	13
Temperate continental forest					6.6	210	0.005	18	29.3	212	0.005	18	6.2	287	0.004	12
Temperate desert					8.7	677	0.005	23	0.5	93	0.006	34	2.2	1523	0.019	76
Temperate mountain system					8	2596	0.026	85	7.2	1129	0.033	94	6.6	1281	0.026	90
Temperate oceanic forest									20.3	179	0.006	25	0.1	226	0.014	63
Temperate steppe					6.2	453	0.004	18	4.1	96	0.003	3	6.7	699	0.003	8
Subtropical desert					2.3	562	0.004	15					2.8	977	0.016	70
Subtropical dry forest	1.3	561	0.018	81	0.2	483	0.026	88	10.8	453	0.018	74	0.2	158	0.011	47
Subtropical humid forest	0.3	469	0.015	86	3.1	429	0.017	69	0.2	238	0.022	72	2.8	89	0.002	2
Subtropical mountain system	1.5	1557	0.017	64	5.6	2574	0.038	96	2.7	1202	0.029	88	1.6	1509	0.027	91
Subtropical steppe	1.7	620	0.009	43	1.9	883	0.017	67	0.1	313	0.056	99	3	942	0.008	33
Tropical desert	30.6	449	0.004	14	4	470	0.006	22								
Tropical dry forest	12.1	644	0.005	23	2.1	248	0.006	26					0.5	543	0.023	81
Tropical moist deciduous forest	15.1	737	0.006	26	2	318	0.014	53					1.6	301	0.016	46
Tropical mountain system	4.8	1549	0.025	87	1.2	1411	0.045	98					0.6	1729	0.043	97
Tropical rainforest	12.8	484	0.005	22	4.1	256	0.018	57					1	415	0.027	75
Tropical shrubland	19.7	611	0.005	18	1.7	353	0.005	18					0.1	376	0.040	100

* percentage of area with a slope superior to the 75 percentile of all the slope observed in the world's land area (≥0.068° at 3 arc-min resolution)

Table S4 (continued).

Oceania				South America			
% of cover	Mean elevation	Mean slope	% of steep slope*	% of cover	Mean elevation	Mean slope	% of steep slope*
2.6	848	0.024	89	0.6	1084	0.037	98
3	348	0.018	73	1.9	417	0.026	87
				3.8	544	0.011	55
48.5	304	0.002	3				
1.6	181	0.005	21	0.7	538	0.022	73
3.5	304	0.013	70	7.5	252	0.004	18
				1.5	2751	0.053	100
18	226	0.003	11	4.2	566	0.010	35
				0.8	788	0.027	89
5	136	0.005	22	9.3	357	0.007	29
0.3	53	0.004	13	23.6	351	0.006	26
0.8	2086	0.062	100	10.3	2627	0.045	93
5	347	0.029	71	35.3	200	0.005	14
11.8	232	0.004	13	0.6	570	0.028	72

References cited in supplementary information:

Amante, C. and Eakins, B. W.: ETOPO1 1 Arc-minute global relief model:procedure, data sources and analysis, National Geophysical Data Center. Marine Geology and Geophysics Division, Boulder, Colorado., 2009.

Chave, J., Andalo, C., Brown, S., Cairns, M., Chambers, J., Eamus, D., Fölster, H., Fromard, F., Higuchi, N., Kira, T., Lescure, J.-P., Nelson, B., Ogawa, H., Puig, H., Riéra, B. and Yamakura, T.: Tree allometry and improved estimation of carbon stocks and balance in tropical forests, Oecologia, 145(1), 87–99, doi:10.1007/s00442-005-0100-x, 2005.

Chave, J., Coomes, D., Jansen, S., Lewis, S. L., Swenson, N. G. and Zanne, A. E.: Towards a worldwide wood economics spectrum, Ecology Letters, 12(4), 351–366, 2009.

FAO: Global Ecological Zoning for the Global Forest Resources Assessment 2000, FAO, Rome., 2001.

Fischer, G., Nachtergaele, F. O., Prieler, S., Teixeira, E., Tóth, G., Velthuizen, H., Verelst, L. and Wiberg, D.: Global Agro-Ecological Zones (GAEZ v3. 0), Laxenburg, Austria: International Institute for Applied Systems Analysis, 2012.

Fenn, K., Malhi, Y., Morecroft, M., Lloyd, C. and Thomas, M.: Comprehensive description of the carbon cycle of an ancient temperate broadleaved woodland, Biogeosciences Discuss., 7(3), 3735–3763, doi:10.5194/bgd-7-3735-2010, 2010.

Jenkins J.C., Chojnacky D.C., Heath L.S. and Birdsey R.A.: National-Scale Biomass Estimators for United States Tree Species, Forest Science, 49(1), 12–35, 2003.

Lutz, J. A., Larson, A. J., Swanson, M. E. and Freund, J. A.: Ecological Importance of Large-Diameter Trees in a Temperate Mixed-Conifer Forest, PLoS ONE, 7(5), e36131, doi:10.1371/journal.pone.0036131, 2012.

Percival, D. P.: On estimation of the wavelet variance, Biometrika, 82(3), 619–631, doi:10.1093/biomet/82.3.619, 1995.

R Development Core Team: R: A language and environment for statistical computing., Vienna, Austria., 2012.

Wang, C.: Biomass allometric equations for 10 co-occurring tree species in Chinese temperate forests, Forest Ecology and Management, 222(1–3), 9–16, doi:10.1016/j.foreco.2005.10.074, 2006.